Desalination and Water Treatment
www.deswater.com

doi: 10.5004/dwt.2023.29144

281 (2023) 265–275
January

Synthesis of a new multi-heterojunction photocatalyst BiOI/Bi_2O_3/MgO and its photocatalytic efficiency in the degradation of Rhodamine B under visible light

Bahia Benalioua[a,*], Imane Benyamina[a], Meriem Mansour[a], Kada Mensri[a], Abdelhadi Bentouami[a], Bruno Boury[b]

[a]*Materials Valorization Laboratory, Abdelhamid Ibn Badis University of Mostaganem, BP 227, Mostaganem 27000, Algeria, email: benalioua.bahia@gmail.com (B. Benalioua)*
[b]*Institut Charles Gerhardt Montpellier, UMR 5253 CNRS-UM-ENSCM, ICGM – UMR 5253, D3, CC 043, 1919, route de Mende 34293 Montepellier cedex 5, France*

Received 3 *October* 2021; Accepted 11 November 2022

ABSTRACT

BiOI/Bi_2O_3/MgO hetero-structured (B/B/M) was prepared by a hydrothermal method and then calcined at different temperatures (200°C, 300°C, 400°C, and 550°C) for 1 h. The efficiency of photocatalyst was tested on the photo-discoloration of a cationic dye (Rhodamine B (RhB)) under visible light (500 W tungsten lamp (Tungsram Trademark) that emits more than 400 nm) and compared to Bi_2O_3, TiO_2-P25 and BiOI as reference photocatalysts. The prepared samples were characterized by X-ray diffraction, Brunauer–Emmett–Teller, UV-Visible diffuse reflectance spectroscopy and scanning electron microscopy. In this new photocatalysts, three structures have been identified BiOI, Bi_2O_3, and MgO before and after heat treatment. Indeed, the sample prepared and calcined at 400°C/1 h show a good crystallinity and display microspheres porous in the form of cauliflower-like. Furthermore, the photocatalytic test of B/B/M-400 has shown efficiency on the photodegradation of RhB. Indeed, a total discoloration of 10 mg/L of RhB was achieved at 110 min.

Keywords: BiOI/Bi_2O_3/MgO; Photocatalyst; Rhodamine B; X-ray diffraction

1. Introduction

Heterogeneous photocatalysis is an advanced oxidation processes (AOP) method that has attracted the attention of several researchers as a technique for elimination refracting and low concentration pollutants from industrial wastewater. These processes are able to transform recalcitrant pollutants into harmless end-products (mineralization to CO_2, H_2O and mineral acids) [1–4]. The heterogeneous photo-catalysis principle is based on the excitation of a semiconductor by irradiation most often the ultraviolet to generate electron-hole pairs. These species react with molecules adsorbed on the surface such as pollutants, oxygen, water, and hydroxyl ions to form radicals such as $O_2^{\bullet-}$ and $OH^{\bullet}$. These radicals have a higher oxidizing potential than traditional oxidants, which are able to partially or totally mineralize most organic compounds [1–4]. The effectiveness of TiO_2 and Evonik Degussa P25 has been shown in several studies in which is still considered as a benchmark in heterogeneous photocatalysis. However, it has two drawbacks: First, its band gap of 3.2 eV limits its photocatalytic activity only under UV. Second, it has a high rate of recombination of electron–hole pairs [4].

* Corresponding author.

Currently, bismuth oxyhalide (BiOX, X = Cl, Br, I) has been used by several researchers [5–7], it has high photocatalytic activity, a narrow band gap (1.77–1.92 eV), and high stability [8,9]. BiOI present a low photocatalytic performance because it has a high recombination of photo-generated e^-/h^+ which is a major drawback. Therefore, the association of two semiconductors in a binary system by combining BiOI with Bi_2O_3 [10,11] further improves the photocatalytic efficiency compared to semiconductor alone. In the literature, many works presenting binary systems such as BiOI/BiOCl [12], BiOI/g-C_3N_4 [13], and ternary systems like α-Bi_2O_3-BiOI-BiOBr [5] with high efficiency compared to semiconductors alone have been reported. Yan et al. [14] have synthesis a multi heterojunction Ag-AgI/BiOI-Bi_2O_3 by solvothermal method, the material showed good photocatalytic results with a 300W xenon lamp with an ultraviolet cut-off filter ($\lambda \geq 420$ nm) on methyl orange (MO) degradation. Zhang et al. [10] have synthesized a binary composite α-Bi_2O_3-BiOI by solvothermal method. The photocatalytic activity of the obtained material has been proven on an antibiotic tetracycline hydrochloride (TC) degradation under visible light of 300 W xenon lamp with an ultraviolet cut-off filter ($\lambda \geq 420$ nm). Kumar et al. [15] synthesized MgO nano powder by bio mediated route. The obtained material has given good photocatalytic discoloration results of Malachite green (MG) and Rhodamine B (RhB) under sunlight irradiation and UV light. These results encouraged us to synthesize a new semiconductor multi-hetero-junction. For such physical and chemical properties as extended specific surface area, wide pore volume size, and thin pore size distribution, thermal and chemical stability and despite its wide band gap [15–19], MgO was chosen to be associated as support for two Bi_2O_3 and BiOI semiconductors. Thus, it seemed interesting to us to target the synthesis of a photocatalyst with a ternary hetero-structure of the BiOI/Bi_2O_3/MgO. To our best knowledge, this structure has never been reported. Our ternary BiOI/Bi_2O_3/MgO composite prepared by the hydrothermal method then calcined at different temperatures has proven its effectiveness especially that calcined at 400°C, in the photo discoloration of RhB compared to semiconductors alone such as BiOI, Bi_2O_3 and TiO_2-P25.

2. Experimental

2.1. Materials

All chemicals were of analytical and were directly used without any treatment. Potassium iodide (KI); bismuth(III) nitrate pentahydrate $Bi(NO_3)_3{\cdot}5H_2O$, $Mg(NO_3)_2{\cdot}6H_2O$, ethylene glycol (EG) ($C_2H_6O_2$), ethanol (C_2H_5OH), distilled water and Rhodamine B (RhB) diethylammonium chloride ($C_{28}H_{31}ClN_2O_3$) were obtained from Sigma-Aldrich company.

2.2. Preparation and characterization

Our photocatalysts was synthesized by solvothermal method. Solution A of $Bi(NO_3)_3{\cdot}5H_2O$ (5.9 mmol, 2.8643 g) was dissolved in 10 mL of EG under ultra-sonication until dissolved. Solution B: 0.6876 g (2.6818 mmol) of $Mg(NO_3)_2{\cdot}6H_2O$ was dissolved in 10 mL of EG using ultrasound apparatus until dissolution. Solution C: 5 mmol of KI was dissolved in 10 mL of EG and left under left in ultrasound apparatus until dissolution. First, solution A was added to solution B and left under stirring for 15 min, the mixture was added drop by drop to solution C under moderate stirring for 1 h. The final mixture was placed in an autoclave and left in the oven at 160°C for 24 h. The reactor was therefore cooled down at room temperature; the obtained material was collected by filtration, washed with distilled water and ethanol then dried at 80°C all night long. The obtained material was calcined at different temperatures (200°C, 300°C, 400°C, and 550°C) for 1 h and named as B/B/M-T where *T* is the calcination temperature; for example, B/B/M-400 is the obtained material calcined at 400°C during 1 h. This synthesis has been illustrated in schematic form in Fig. 1.

2.3. Effect of calcination temperature

The test consists in determining the optimal calcination temperature of material for better photocatalytic activity. The heat treatment was performed in a muffle furnace at different temperatures (200°C, 300°C, 400°C, and 550°C) during 1 h. The photocatalytic efficiency was evaluated with 100 mg of each material in 100 mL of RhB aqueous solution at 10 mg/L. The suspension was magnetically stirred and exposed to visible light. The result in the form of percentage of photo-discoloration was determined after separation by centrifugation and analysis of the supernatant by spectrophotometry at 553 nm using a JASCO V-730 UV-Visible spectrophotometer. The discoloration yield was determined by the Eq. (1).

$$\%\text{yield} = \frac{Abs_t - Abs_0}{Abs_0} \times 100 \quad (1)$$

2.4. Adsorption kinetics

The adsorption kinetics tests were performed using 0.5 g of B/B/M-400 in 500 mL of aqueous solution of RhB at 10 mg/L. The suspension was stirred in the dark during 2 h at natural pH 5.65 and at room temperature with respect to solid/solution ratio of 1 g/L. Samples were taken at regular time and centrifuged. Equilibrium dye concentrations in the supernatants were analyzed at 553 nm using a JASCO V-730 UV-Visible spectrophotometer. A calibration curve in the range of 1–10 mg/L of the RhB solution has been established. The RhB adsorption kinetics experiments were repeated three times to obtain the average results.

2.5. Photocatalytic test

2.5.1. Direct photolysis

This study was carried out without photocatalyst in order to verify the stability of RhB under visible light irradiation. For this, 100 mL of 4 mg/L of RhB solution at natural pH 5.65 and at room temperature was stirred and exposed to visible light irradiation. Aliquots of approximately 5 mL were sampled after every 10 min and analyzed as above.

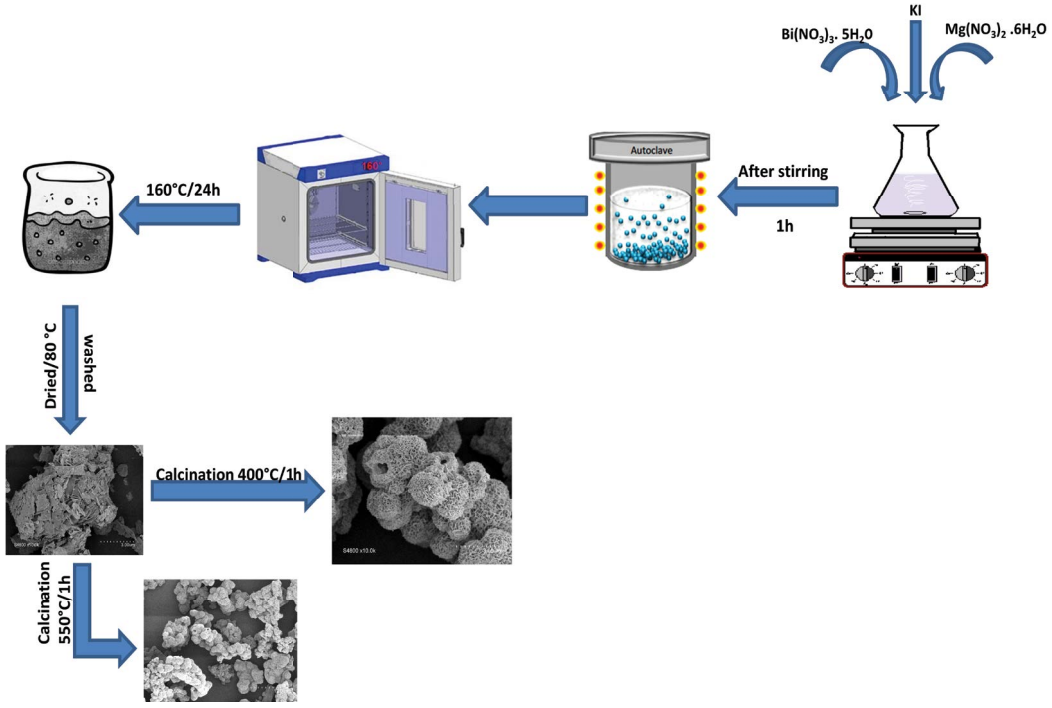

Scheme 1. Schematic for preparation of sample.

2.5.2. In the presence of the photocatalyst

The photo-discoloration kinetics of RhB in the presence of the B/B/M-400 with a solid/solution ratio of 1 g/L was carried out in 100 mL of dye solution at different concentration between 2 and 10 mg/L, at natural pH 5.65 and at room temperature. Once the adsorption–desorption equilibrium was reached after 60 min, the stirred suspension was exposed to visible light supplied by a 500 W tungsten lamp (Tungsram Trademark) emitting more than 400 nm and it was used without a cut-off filter. The characteristics of the lamp have been carefully presented in our previous works [20]. An adsorption, in the dark during the equilibrium time, should be performed. Once the equilibrium time is reached, the lamp is turned on. Samples were taken at regular times, separated by centrifugation and the residual dye concentrations in the supernatants were determined by spectrophotometry as above. The RhB photo-discoloration kinetics experiments were repeated three times to obtain the average results.

2.6. Active species identification

Four radical species (e^-, h^+, $OH^\bullet$ and $O_2^{\bullet-}$) can be involved directly or indirectly in the photodegradation of organic pollutants. To elucidate the responsible active species and their contribution in the degradation of RhB, different active species inhibitors are used. In this study, ascorbic acid (2 mmol/L) is used as a scavenger of the $O_2^{\bullet-}$ radical anion, *t*-butanol (2 mmol/L) as an inhibitor of hydroxyl radicals ($OH^\bullet$), Na_2EDTA (1 mmol/L) as a scavenger of h^+ and $K_2Cr_2O_7$ (1 mmol/L) as e^- acceptor [5,6,20–22]. The identification of active species was carried out at 4 mg/L of RhB at pH 5.65 and at solid/solution ratio of 1 g/L in the presence of each scavenger. Samples were taken at regular time, centrifuged, and the concentration of dye in the supernatant was determined as above.

2.7. Reusability study

In order to assess the stability and longevity of the prepared photocatalyst (B/B/M-400) photo-discoloration study of 10 mg/L RhB solution was carried out at natural pH 5.68 with photocatalyst concentration of 1 g/L. The suspension was stirred for 60 min in dark then exposed to visible light until complete discoloration for 120 min. The photocatalyst was separated by centrifugation and dried without washing in the oven at 110°C for 2 h. Then the material was added in a new solution of RhB at the same concentration as the first. The process of reusing the material was repeated four times.

3. Results and discussions

3.1. Characterization

3.1.1. X-ray diffraction analysis

X-ray diffraction analysis was performed to determine the purity and structure of the phases present. The diffractograms (Fig. 2) of uncalcined and calcined material at 400°C and 550°C have three different phases BiOI, Bi_2O_3, and MgO. Indeed, values of 2θ equal to 9.61°, 31.61°, 49.91°, and 55.33°, which can be attributed to the d_{001}, d_{110}, d_{202}, and d_{212}, respectively for the BiOI phase (tetragonal phase, space group P4/nmm) ($a = b$ = 3.9840 Å, c = 9.1280 JCPDS

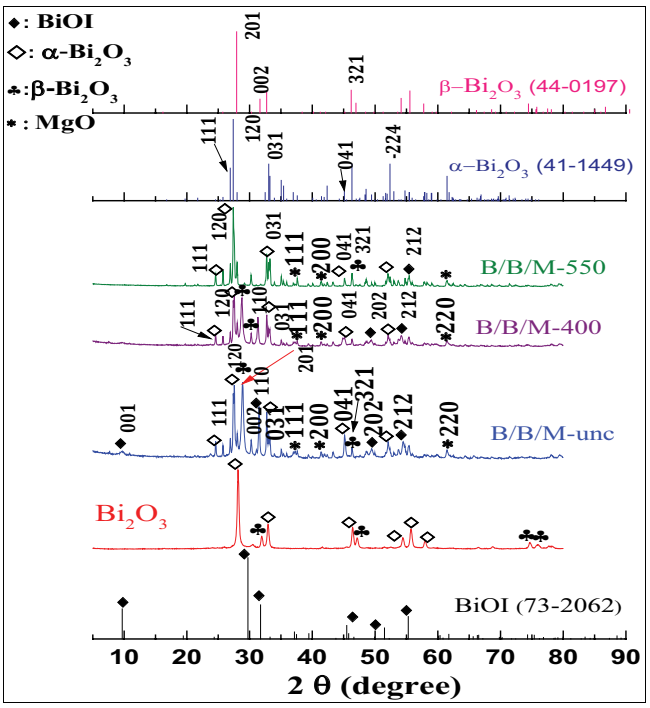

Fig. 2. X-ray diffraction pattern of BiOI-Bi_2O_3-MgO uncalcined and calcined materials.

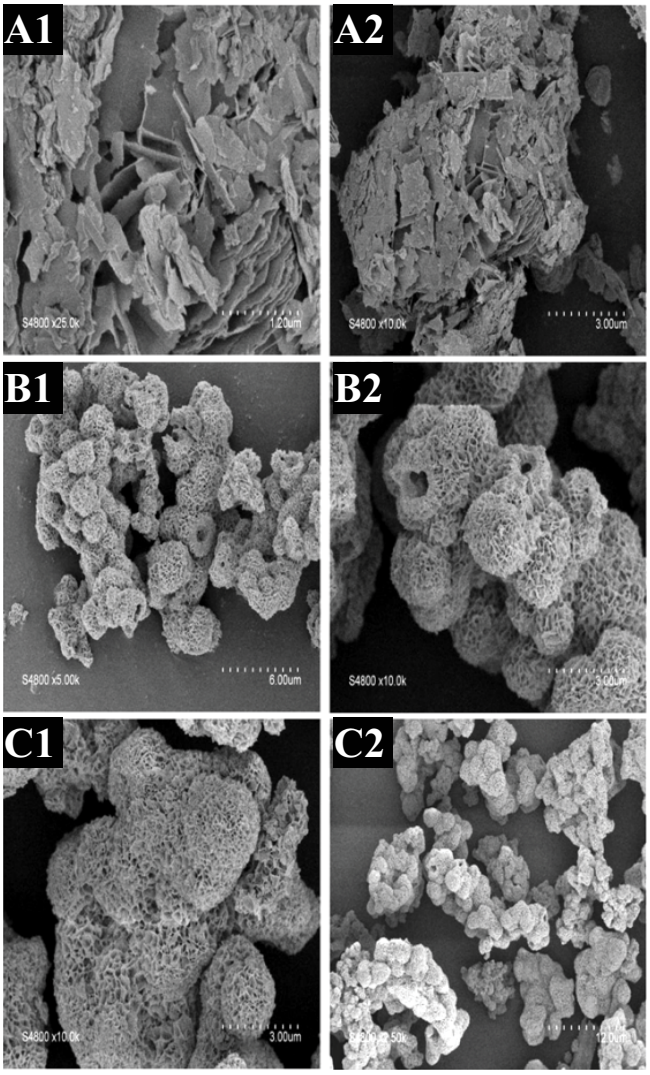

Fig. 3. SEM images of BiOI-Bi_2O_3-MgO composites uncalcined and calcined materials.

73-2062) [23,24]. According to the X-ray diffraction (XRD) pattern, the BiOI phase appeared only for the uncalcined and calcined material at 400°C. According to the literature the element iodine begins to disappear by volatilization from 340°C [25]. For material B/B/M-550 the BiOI phase completely disappears due to the probable volatilization of iodine. In addition, an α-Bi_2O_3 (monoclinic phase, space group P21/c) phase (JCPDS41-1449) [5,26,27] was identified according to peaks at 26.92°, 27.37°, 35.40°, 46.32°, and 55.44° that can be attributed to the (111), (120), (031), (041), and (–224) plane respectively.

The results also indicate the presence of the tetragonal phase peaks of β-Bi_2O_3 which are at position 28.15°, 31.38°, 45.19° and which correspond to (201), (220), (321) of the crystal planes (space group P-421/c) (JCPDS44-0197) [28] respectively. Furthermore, it is also noted that the presence of 2θ values: 36.9° and 43.2° correspond to the (111), and (200) reflection respectively for the cubic phase of MgO (space group Fm-3m) ($a = b = c = 4.20$ Å) (JCPDS 87-0653) [15].

3.1.2. Scanning electron microscopy analysis

The morphology evolution of B/B/M calcined and uncalcined materials are shown in Fig. 3. The images of uncalcined materials (Fig. 3A1-A2) show a formation of sand-rose with smooth nanosheets and a few fragments of petals probably those of the composite BiOI. For calcined materials at 400°C/1 h, scanning electron microscopy (SEM) images (Fig. 3B1-B2) show microspheres porous in the form of cauliflower-Like are composed of lots nanosheets, and whose shape of these nanosheets has slightly decreased compared to those of calcined material at 550°C (Fig. 3C1-C2).

3.1.3. N_2 adsorption–desorption analysis

The specific surface area and pore size distribution of the prepared samples was determined by Brunauer–Emmett–Teller method from the adsorption isotherm of nitrogen gas at 77 K which belongs to the type IV category, (Fig. 4A). The values of specific surface area pore diameter and pore volume are presented in Table 1. From the results, it appears that the specific surface of the non-calcined material (B/B/M-Unc) at 44.57 m^2/g is greater than that of the material calcined at 400°C at 21.48 m^2/g. Moreover, the non-calcined material displays a micro-porosity against a macro-porosity for the calcined. Thus, the heat treatment increased the pore size probably due to the evaporation of the residual organic solvent and part of the iodine and reduced the pore volume (inset Fig. 4A). The pore volume of B/B/M-Unc is higher than that of B/B/M-400; it decreases from 0.2822 to 0.2053 cm^3/g, respectively. It is noted that the specific surface area of B/B/M decreases with the increase of calcination temperature

which can be explained by the growth of crystallite size which can be beneficial in the photocatalytic property [29]. This observed decrease in the specific surface is probably due to the evaporation of the rest of the solvent used in the synthesis on the one hand and to the partial disappearance of the iodine on the other hand from the BiOI phase as indicated in the XRD results.

3.1.4. UV-Vis diffuse reflectance spectroscopy

The optical properties and the bandgap energy (E_g) of semiconductors are important factors in determining the performance of photocatalysts. The UV-Visible diffuse reflectance spectroscopy (DRS) analysis was carried out only on the material which gave the best efficiency named B/B/M-400. The bandgap energy can be determined from the Tauc equation given by the following formula:

$$(\alpha h\nu) = \beta\left(h\nu - E_g\right)^n \quad (2)$$

where h, ν, and β are the Planck's constant (J/s), the light frequency (s^{-1}) and the proportionality coefficient respectively. The n value depends on the electronic transition type between the valence and conduction bands and can be 1/2 or 2 for a direct or indirect transition respectively.

The value of E_g of the prepared material B/B/M-400°C was determined from the plot (Fig. 4B) of the modified Tauc function which is given in the Eq. (3):

$$(\alpha h\nu)^{1/n} = \beta\left(h\nu - E_g\right) \quad (3)$$

The absorption coefficient α is linked to the Kubelka–Munk (K-M) function by diffuse reflectance R according to the Eq. (4):

$$F(R) = \frac{(1-R)^2}{2R} \approx \frac{\alpha}{s} \quad (4)$$

where α and s are the absorption and scattering coefficients respectively.

Comparing the studies that have been done by several researchers [5–8] on the determination of the bandgap energy (E_g) it has been shown that the electronic transition is direct for B/B/M-400, and the latter has been verified by calculating the bandgap energy (E_g) from the modified K-M equation. Plotting $(\alpha h\nu)^2$ as a function of $h\nu$ allowed us to determine the bandgap energy of the calcined material (B/B/M-400) and its value was 2.53 eV. So based on this value, it can be said that the calcined material could be photoactive under visible light.

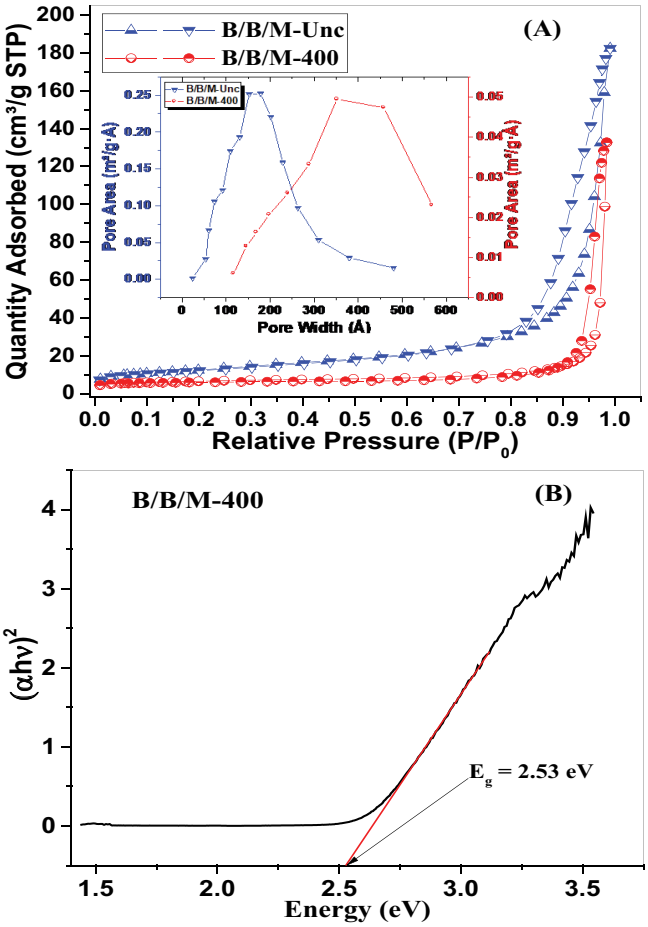

Fig. 4. (A) N_2 adsorption–desorption isotherms of B/B/M uncalcined and calcined at 400°C and (B) Tauc plot from UV-Visible DRS of B/B/M-400.

3.2. Effect of heat treatment temperature

The photocatalytic efficiency of the prepared material as a function of calcination temperature is plotted as a histogram in Fig. 5A. It appears from the graph that the efficiency increases with the temperature until 400°C, beyond this temperature, the efficiency drops. Indeed, a photodiscoloration yield of 20.49 was achieved for the non-calcined; and 79.30%, 89.25%, 100% and 56.66% were obtained

Table 1
Textural and optical properties of prepared composites obtained from adsorption–desorption of N_2 at 77 K

Sample	C_i (mg/L)	$C_{i,corr}$ (mg/L)	K_{app} (min^{-1})	V_0 (mg/L·min)	R^2
B/B/M (400°C)	2.0	1.32888	0.015	0.01993	0.9038
	4.0	3.32694	0.013	0.04325	0.9826
	6.0	5.26806	0.011	0.05794	0.9830
	8.0	7.87836	0.009	0.07090	0.9851
	10.0	9.7787	0.006	0.09098	0.9972

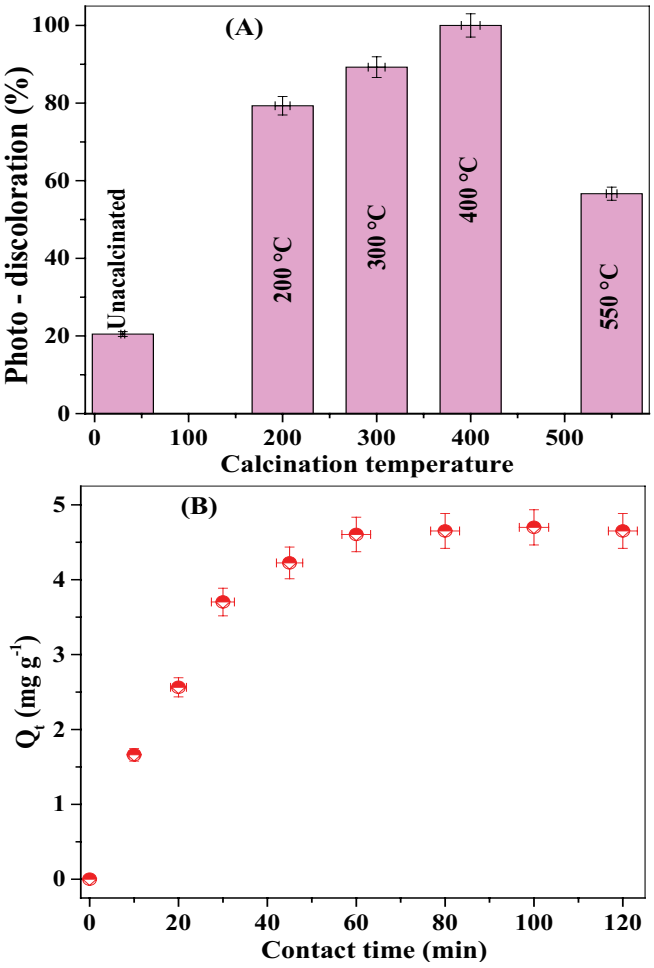

Fig. 5. (A) Effect of calcination temperature on the rate of photo-discoloration of RhB and (B) adsorption kinetics of RhB on B/B/M-400 (C_i = 10 mg/L; pH_i = 5.65; 1 g/L of solid/solution ratio).

for those treated at 200°C, 300°C, 400°C and 550°C respectively. This is due to the opening of the pores, indeed, after calcination, the material presents a macroporosity against microporosity for the uncalcined and this despite of a low specific surface for the calcined. At 550°C the BiOI phase has completely disappeared, which has caused a reduction in the photocatalytic yield.

3.3. Determination of the equilibrium time

The results of the adsorption kinetics of RhB by the B/B/M-400 material are plotted in Fig. 5B. From the plots, it appears that the adsorption of RhB is fast with our material. Indeed, the equilibrium is reached after 60 min. Moreover, the maximum amount of adsorbed dye by B/B/M-400 is 4.60 mg/g. In the literature, it has been noted that the adsorption capacity of certain photocatalysts towards RhB depends on the concentration of RhB but above all on the surface properties of the photocatalyst. By way of example, some results from the literature [5,30] relating to the maximum adsorption capacity in comparison with that of this study are shown in Table 2.

Table 2
Comparative values of maximal adsorption capacity of some photocatalysts towards RhB

Photocatalyst	[RhB] (mg/L)	Q_{max} (mg/g)	References
S-PVP	40	27	[5]
S-PVP-GW	40	20	[5]
BiOBr	50	42.14	[30]
BiOI-Bi_2O_3-MgO	10	4.60	This study

3.4. Photo-discoloration study of RhB

3.4.1. Comparative study

The comparison of the photocatalytic efficiency between the B/B/M-400 and other photocatalysts is shown as a histogram in Fig. 6. First, it appears from the histogram that the direct photolysis (without material) of 4 mg/L of RhB is almost negligible. Indeed, about 10% yield was obtained after 120 min and remains unchanged even after 3 h of irradiation. Exactly and at 10 mg/L of RhB aqueous solution, 100% of discoloration with B/B/M-400 was attained after 110 min. While, during the same time, yield of 33.78%, 27.80% and 77.51% were obtained with Bi_2O_3; BiOI and TiO_2-P25 respectively. Otherwise, with the material B/B/M-550 a very poor photocatalytic yield was obtained at the same dye concentration and during the same time. This is possibly due to the absence of the BiOI phase of the material as a consequence of the probable total volatilization of iodine at 550°C.

3.4.2. Kinetics of the photo-discoloration

In this part, the study was carried out only in the presence of the best photocatalyst named B/B/M-400. The plot of the C_i/C_t ratio of the photo-discoloration kinetics of RhB at different concentration as a function of time is presented in Fig. 7A. First, it emerges from the graph that RhB is more or less resistant to visible light irradiation without photocatalyst. In fact, a photo-discoloration yield of »10% was achieved after 120 min under visible light irradiation. This poor yield of discoloration remained unchanged even after 180 min. Secondly, with B/B/M-400, photo-discoloration of RhB was evaluated by varying the dye concentration from 2 to 10 mg/L at natural pH 5.65. The plotted curves show that for each dye concentration, photo-discoloration is fast and efficient with B/B/M-400 compared to reference photocatalysts. For indication, in the case of a concentration of 10 mg/L for example, 100% discoloration was obtained after 110 min of irradiation under visible light. Six studies [31–36] were chosen and reported in Table 3 for comparison between their results and those of this present work.

3.4.3. Modeling the kinetics of photodegradation

Modeling of pseudo-first-order model, which may be applied on a linear form indicated by Eq. (5), can be used to characterize the kinetics of the photodegradation rate of most organic molecules.

$$\ln\frac{C_{i,\text{corr}}}{C_t} = K_{\text{app}}t \quad (5)$$

where k_{app} is the apparent rate constant, $C_{i,corr}$ (corrected initial concentration after dark adsorption) and C_t is the concentration at time t. Plots of $\ln(C_{i,corr}/C_t)$ vs. reaction time are shown in Fig. 7B. The photocatalytic discoloration kinetic data had been in good agreement with the pseudo-first-order kinetics based on the good correlation coefficient values ($R^2 > 0.9568$), for dye concentrations ranging from 2 to 10 mg/L. Table 4 displays the kinetic constants values (k_{app}) and rate of initial concentration V_i at different initial RhB concentrations with the solid/solution ratio of 1 g/L and natural pH of the solution 5.65. It can be observed that the initial velocity increases with the increase of the initial dye concentration with correlation coefficient values R^2 higher than 0.903 in the range 2–10 mg/L of initial dye concentration. From Table 4 it can be seen that there is a relationship between the initial photo-discoloration rate and the initial RhB concentration. This relationship can be successfully represented by the Langmuir–Hinshelwood kinetic model used for heterogeneous photocatalytic degradation [20,37,38] and expressed by Eq. (6).

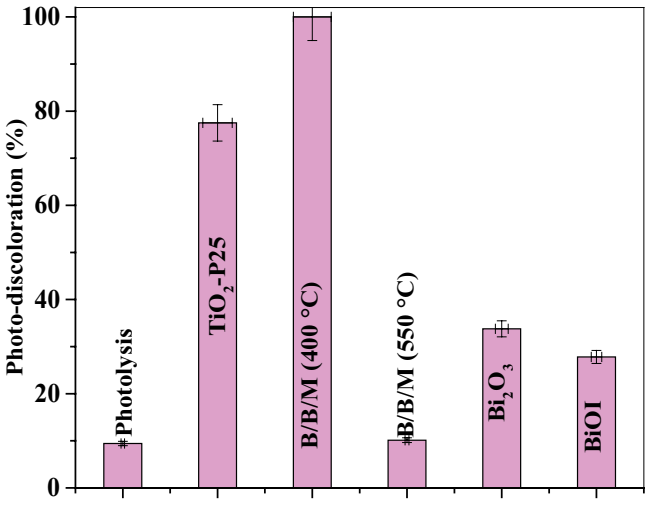

Fig. 6. Comparative study between prepared materials uncalcined and calcined at different temperature and benchmark photocatalysts on photo-discoloration of RhB at 10 mg/L under visible light.

$$V_i = K_{\text{app}}C_{i,\text{corr}} = \frac{K_{\text{ads}}K_{L-H}C_{i,\text{corr}}}{1+K_{L-H}C_{i,\text{corr}}} \quad (6)$$

Eq. (7) was determined after the linearization of Eq. (6). It shows the correlation between $1/V_i$ and $1/C_{i,corr}$.

$$\frac{1}{V_i} = \frac{1}{K_{L-H}} + \frac{1}{K_{L-H}K_{\text{ads}}} \times \frac{1}{C_{i,\text{corr}}} \quad (7)$$

where V_i (mg/L·min) is the initial rate of the photocatalytic discoloration, $K_{L–H}$ (mg/L·min) is the Langmuir–Hinshelwood rate constant, K_{ads} is the adsorption equilibrium constant on photocatalyst in (mg/L), and $C_{i,corr}$ is the initial dye concentration corrected after adsorption in dark (mg/L). The inverse of the initial rate as a function of the inverse of the corrected initial dye concentration is shown in Fig. 8. According to the figure, the curve is linear and indicates that the photocatalytic reaction follows the Langmuir–Hinshelwood model. The values of the rate constant $K_{L–H}$ (0.189 mg/L·min) and the adsorption equilibrium constant K_{ads} (0.082 L/mg) were determined from the slopes of Fig. 8. First observation made is that the value of the constant $K_{L–H}$ is significantly higher than that of K_{ads}. This result is frequently observed in the literature, several hypotheses have been put forward to explain this difference. Lin et al. [39] assume that this increase in $K_{L–H}$ is due to photo-adsorption, whereas according to Cunningham and Al-Sayyed [40], the photodegradation reaction takes place not only on the surface but also in solution.

3.4.4. Active species identification

The superoxide $O_2^{\bullet-}$, $HO^{\bullet}$ radicals, holes and electrons photo-generated are active species that contribute mutually or individually in the photocatalytic degradation of organic pollutants. The addition of scavengers (active species inhibitors) has been proposed to identify the responsibility of each species on dye degradation [21,22]. Fig. 9 shows the role of different scavenger effect on the efficiency of photocatalytic discoloration of RhB by B/B/M-400 under visible light. A complete discoloration was obtained after 110 min without any scavengers. The addition of Na_2EDTA (as h^+ scavenger) decreases the rate of discoloration. Indeed after 110 min of

Table 3
Comparison between this present work with the reported literature studied so far using different light sources

Photocatalyst	[RhB]	Light source (power or irradiance)	% degradation (time)	References
α/β-Bi_2O_3	10 mg/L	Visible (9 Watt with irradiance of 33 W/m^2)	80 (210 min)	[31]
Bi_2O_3 nanofibers	20 mg/L	UV-A	95 (120 min)	[32]
α-Bi_2O_3	20 mg/L	Xe (300 W)	36 (60 min)	[33]
Bi_2O_3/BiOCl			100 (60 min)	
α/β-Bi_2O_3	10 ppm	Natural sunlight	89 (120 min)	[34]
α/β-Bi_2O_3	10^{-5} M	Natural sunlight	99.7 (180 min)	[35]
Bi_2O_3 nanoflakes	10^{-5} M	Xe (500 W)	90% (5 h)	[36]
BiOI/Bi_2O_3/MgO	10 mg/L	Visible light tungsten (500 W)	100 (110 min)	This work

irradiation only 43.26% was obtained. Furthermore, about 89.20% of discoloration was achieved during the same irradiation time when ascorbic acid (as superoxide scavengers) was used. In addition, the presence of $K_2Cr_2O_7$ (as e^- scavenger) causes a small decrease in photo-discoloration rate when compared to the case without scavengers. However, full discoloration was obtained within 60 min when *t*-butanol (as a scavenger of $OH^•$) was used; but strong adsorption of the dye in the dark was observed which aided probably this rapidity in the photo-discoloration of RhB after 60 min. This result indicates that h^+ is the active species predominantly responsible for the discoloration with a moderate and minimal contribution of $O_2^{•-}$ and e^-, respectively.

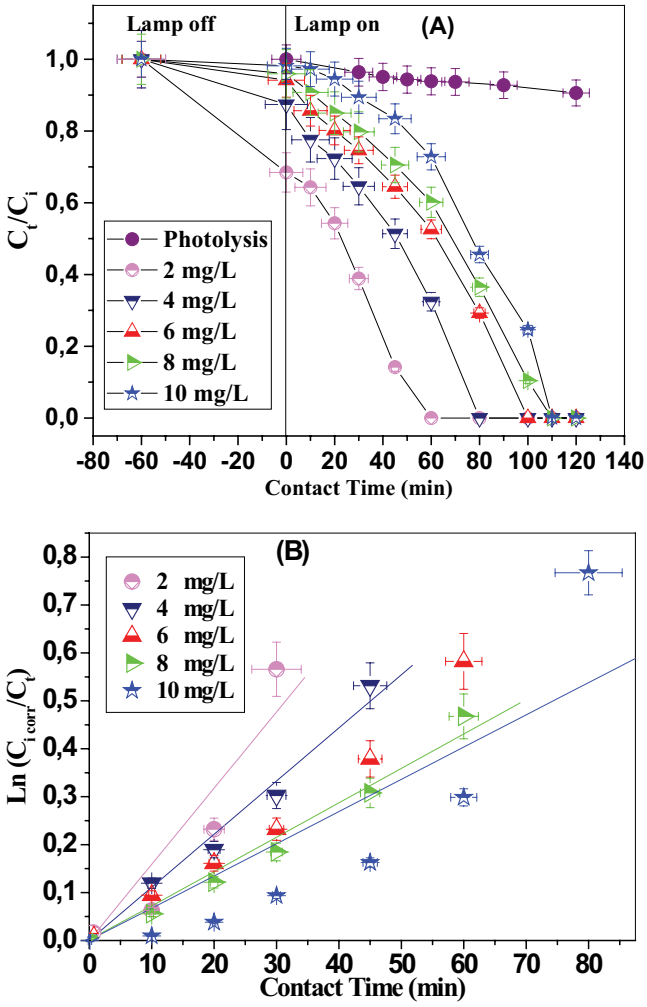

Fig. 7. (A) Photo-discoloration kinetics of RhB by B/B/M-400 at different concentrations and (B) application of the pseudo-first-order kinetic model to the photo-discoloration of RhB.

3.4.5. Photocatalytic reaction mechanism

The reaction mechanism of the photocatalytic discoloration of RhB by the photocatalyst has been proposed in Fig. 10. Firstly, the location of the valence and conduction bands edge of BiOI, Bi_2O_3, and MgO were calculated by Mulliken electronegativity theory via Eqs. (8) and (9) [5,41,42]:

$$E_{VB} = \chi - E_C + 0,5E_g \quad (8)$$

$$E_{CB} = E_g - E_{VB} \quad (9)$$

where E_C is the energy of free electrons on the scale of hydrogen, around 4.5 eV. And χ is the absolute electronegativity of the samples. Indeed, the value of χ of BiOI, Bi_2O_3, and MgO are respectively 5.99, 6.23, and 4.75 eV, that are close to those found in the literature [11,43,44]. According

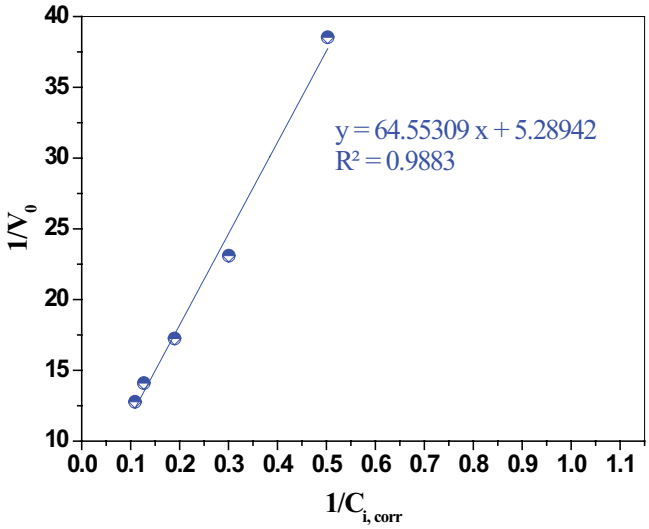

Fig. 8. Langmuir–Hinshelwood kinetic model plots of RhB photo-discoloration under visible light by B/B/M-400 (pH_i = 5.65; solid/solution ratio = 1 g/L).

Table 4
Kinetics parameters of RhB photo-discoloration at different initial dye concentration under visible light

Photocatalyst	C_i (mg/L)	$C_{i,corr}$ (mg/L)	K_{app} (min^{-1})	V_i (mg/L·min)	R^2
B/B/M (400°C)	2.0	1.73	0.015	0.02595	0.9038
	4.0	3.33	0.013	0.0433	0.9826
	6.0	5.27	0.011	0.0579	0.9830
	8.0	7.88	0.009	0.0709	0.9851
	10.0	9.78	0.008	0.07824	0.9972

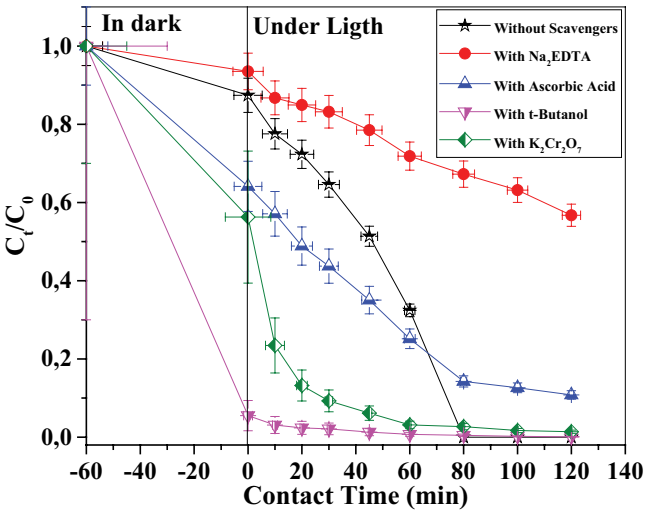

Fig. 9. Identification of the active species with different scavengers on the photocatalytic discoloration of RhB under visible light in the presence of B/B/M-400.

to Eqs. (8) and (9); the value of E_{VB} and E_{CB} are respectively 2.42 and 0.56 eV for BiOI; 3.08 and 0.37 eV for Bi_2O_3, and 2.42 and –1.92 eV for MgO.

The energy of the photons (E_g < 3.2 eV) coming from the visible lamp (λ > 400 nm) is greater than that of the band gap of the photocatalysts of BiOI (1.86 eV) and Bi_2O_3 (2.71 eV) [11]. Thus, electrons from VB of BiOI (2.42 eV) and Bi_2O_3 (3.08 eV) are excited and should be transferred to the CB of BiOI (0.56 eV) and/or Bi_2O_3 (0.37 eV) thus forming pairs e^-/h^+ (reaction 1). Photon energy from the visible lamp can stimulate valence band electrons to the most negative energy level (BiOI −0.68 eV, and Bi_2O_3 −0.13eV). Since the energy level of CB of Bi_2O_3 is higher than that of BiOI, the e^- should move from the CB of BiOI to CB of Bi_2O_3. The latter is also lower than the energy level of the couple $O_2/O_2^{\bullet-}$ (−0.046 eV NHE) [45,46]. Thus, the CB of BiOI and that of Bi_2O_3 are considered as electron donors to dissolved oxygen. Accordingly, the dissolved oxygen should react with the electrons of CB to give the superoxide anion radical (reaction 2).

Otherwise, the difference energy between LUMO (−1.42 eV) and HOMO (0.95 eV) of RhB [47] is lower than the photon energy of visible light (E_g < 3.2 eV), the transition of the RhB electrons occurs to form RhB* (reaction 3). In fact, an electron jumps from LUMO to the CB of Bi_2O_3 and/or BiOI to give RhB^+ (reaction 4). And as the valence band energy of Bi_2O_3 is higher than that of BiOI. Moreover, the holes of VB of Bi_2O_3 can be transferred to the VB of BiOI.

Regarding the production of free radicals, as the VB energy of BiOI is higher than that of $OH^-/OH^\bullet$ (1.99 eV) [48] the hole (h^+) at VB of BiOI should react with H_2O molecules to give radical $OH^\bullet$ (reaction 5). While e^- can be delivered by the CB of MgO (reaction 6). The latter can react with dissolved oxygen to form $O_2^{\bullet-}$ (reaction 7). Then, the radical formed can probably react with H^+ protons to give H_2O_2 (O_2/H_2O_2, 0.682 eV) [49] (reaction 8). These radicals ($OH^\bullet$, $O_2^{\bullet-}$, H_2O_2) can lead to the mineralization of the RhB into small molecules (reaction 9).

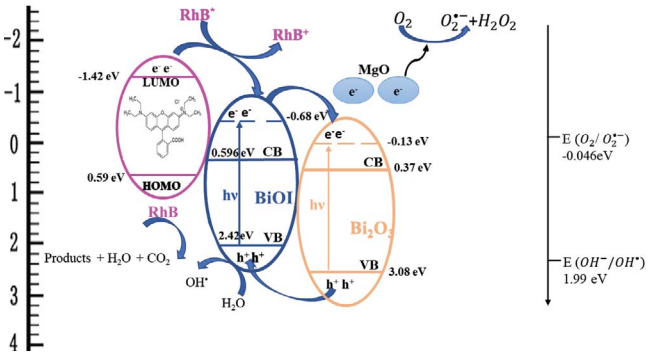

Fig. 10. Proposed mechanism of the photocatalytic discoloration of RhB by BiOI/Bi_2O_3/MgO under visible light.

The recombination of electron/hole pairs at the B/B/M-400 (BiOI/Bi_2O_3/MgO-400) heterojunction interface is slow which gives a high photocatalytic performance (reaction 10). As a result, an association of reactions describes the mechanism of photodegradation of RhB by the B/B/M-400 (BiOI/Bi_2O_3/MgO-400):

$$BiOI-Bi_2O_3-MgO+h\nu \rightarrow BiOI-Bi_2O_3-MgO\left(e^-+h^+\right) \quad \text{(I)}$$

$$e^-+O_2 \rightarrow O_2^{\bullet-} \quad \text{(II)}$$

$$RhB+h\nu \rightarrow RhB^* \quad \text{(III)}$$

$$RhB^*+CB \rightarrow RhB^+ \quad \text{(IV)}$$

$$BiOI-Bi_2O_3\left(h^+\right)+H_2O \rightarrow BiOI-Bi_2O_3+H^++HO^\bullet \quad \text{(V)}$$

$$BiOI-Bi_2O_3\left(e^-\right)+MgO \rightarrow BiOI+Bi_2O_3+MgO\left(e^-\right) \quad \text{(VI)}$$

$$MgO\left(e^-\right)+O_2 \rightarrow O_2^{\bullet-}+MgO \quad \text{(VII)}$$

$$2O_2^{\bullet-}+2H^+ \rightarrow O_2+H_2O_2 \quad \text{(VIII)}$$

$$RhB^++HO^\bullet+O_2^{\bullet-} \rightarrow \text{intermediates}+CO_2+H_2O+\text{Products} \quad \text{(IX)}$$

$$h^++e^- \rightarrow \text{heat}\left(\text{slow reaction}\right) \quad \text{(X)}$$

3.4.6. Photocatalyst regeneration

The stability of B/B/M-400 was evaluated after four uses (Fig. 11). From the fourth use a small decline in photocatalytic efficiency of about 3.5% was observed after 110 min. This could confirm that the recombination of the e^-/h^+ pair of the new hetero-structured photocatalyst is negligible. The B/B/M-400 photocatalyst can be judged to have stability and preserve its photocatalytic efficiency after 4 uses and maybe more.

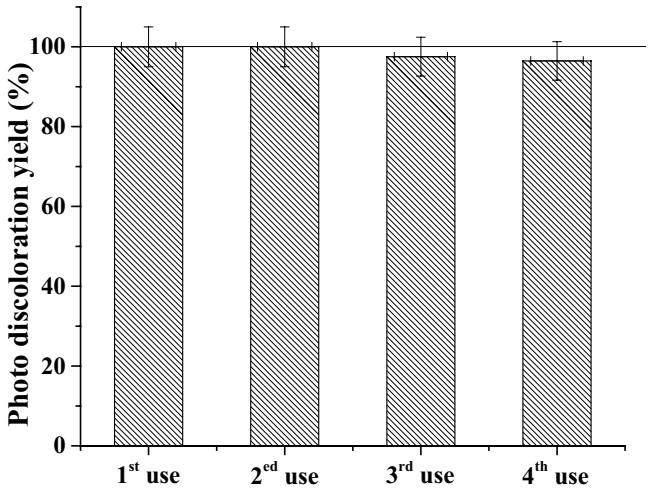

Fig. 11. Reuses and stability performance of B/B/M-400.

4. Conclusion

A Bi_2O_3/BiOI/MgO hetero-structured ternary material was prepared by the hydrothermal route followed by a heat treatment at different temperatures. The heat treatment of the material obtained has made it possible to increase the photocatalytic efficiency but beyond 400°C, this efficiency drops. The efficiency obtained with the material treated at 400°C is probably due to the presence of the three structures BiOI, Bi_2O_3 and MgO in adequate proportions. Each brings its contribution thanks to its properties. The heat treatment plays an important role in the restructuring of the phases but can also destroy certain phases, for example the volatilization of certain atoms such as the halogens (here the iodine which begins to volatilize from 400°C). However, the combination of the three therefore reduced iodine volatilization and promoted the efficiency of the three semiconductors over the efficiency of each alone. This new combined photocatalyst could be a good candidate in the treatment of polluted water.

Acknowledgements

This work is part of a project (A16N01UN270120200005) funded by the thematic science and technology research agency (ATRSDT) of the general direction of scientific research and technological development (DGRSDT) within the Algerian ministry of higher education and scientific research.

References

[1] M.R. Hoffmann, S.T. Martin, W. Choi, D.W. Bahnemann, Environmental applications of semiconductor photocatalysis, Chem. Rev., 95 (1995) 69–96.
[2] I.A. Alaton, I.A. Balcioglu, D.W. Bahnemann, Advanced oxidation of a reactive dyebath effluent: comparison of O_3, H_2O_2/UV-C and TiO_2/UV-A processes, Water Res., 36 (2002) 1143–1154.
[3] I.K. Konstantinou, T.A. Albanis, TiO_2-assisted photocatalytic degradation of azo dyes in aqueous solution: kinetic and mechanistic investigations: a review, Appl. Catal., B, 49 (2004) 1–14.
[4] C. Sahoo, A. Gupta, A. Pal, Photocatalytic degradation of Crystal Violet (CI Basic Violet 3) on silver ion doped TiO_2, Dyes Pigm., 66 (2005) 189–196.
[5] M. Mansour, I. Benyamina, B. Benalioua, A. Bentouami, B. Boury, H. Hentit, P.-E. Lippens, Combined effect between PVP and glass wool for improvement of the photocatalytic activity under visible light of bismuth(III) oxyhalide and access to α-Bi_2O_3-BiOI-BiOBr, Appl. Surf. Sci., 534 (2020) 147577, doi: 10.1016/j.apsusc.2020.147577.
[6] I. Benyamina, K. Manseri, M. Mansour, B. Benalioua, A. Bentouami, B. Boury, New Bi_2O_3-ZnO composite deposited on glass wool. Effect of the synthesis method on photocatalytic efficiency under visible light, Appl. Surf. Sci., 483 (2019) 859–869.
[7] K. Natarajan, H.C. Bajaj, R.J. Tayade, Photocatalytic efficiency of bismuth oxyhalide (Br, Cl and I) nanoplates for RhB dye degradation under LED irradiation, J. Ind. Eng. Chem., 34 (2016) 146–156.
[8] X. Wang, Y. Zhang, C. Zhou, D. Huo, R. Zhang, L. Wang, Hydroxyl-regulated BiOI nanosheets with a highly positive valence band maximum for improved visible-light photocatalytic performance, Appl. Catal., B, 268 (2020) 118390, doi: 10.1016/j.apcatb.2019.118390.
[9] D. Sun, J. Li, L. He, B. Zhao, T. Wang, R. Li, S. Yin, Z. Feng, T. Sato, Facile solvothermal synthesis of BiOCl-TiO_2 heterostructures with enhanced photocatalytic activity, CrystEngComm, 16 (2014) 7564–7574.
[10] P. Zhang, H. Liu, H. Liang, J. Bai, C. Li, Enhanced charge separation of α-Bi_2O_3-BiOI hollow nanotube for photodegradation antibiotic under visible light, Chem. Res. Chin. Univ., 36 (2020) 1227–1233.
[11] Y. Li, J. Wang, H. Yao, L. Dang, Z. Li, Chemical etching preparation of BiOI/Bi_2O_3 heterostructures with enhanced photocatalytic activities, Catal. Commun., 12 (2011) 660–664.
[12] L. Sun, L. Xiang, X. Zhao, C.-J. Jia, J. Yang, Z. Jin, X. Cheng, W. Fan, Enhanced visible-light photocatalytic activity of BiOI/BiOCl heterojunctions: key role of crystal facet combination, ACS Catal., 5 (2015) 3540–3551.
[13] J.-C. Wang, H.-C. Yao, Z.-Y. Fan, L. Zhang, J.-S. Wang, S.-Q. Zang, Z.-J. Li, Indirect Z-scheme BiOI/g-C_3N_4 photocatalysts with enhanced photoreduction CO_2 activity under visible light irradiation, ACS Appl. Mater. Interfaces, 8 (2016) 3765–3775.
[14] Q. Yan, X. Xie, Y. Liu, S. Wang, M. Zhang, Y. Chen, Y. Si, Constructing a new Z-scheme multi-heterojunction photocataslyts Ag-AgI/BiOI-Bi_2O_3 with enhanced photocatalytic activity, J. Hazard. Mater., 371 (2019) 304–315.
[15] M.A. Kumar, B. Mahendra, H. Nagaswarupa, B. Surendra, C. Ravikumar, K. Shetty, Photocatalytic studies of MgO nano powder; synthesized by green mediated route, Mater. Today:. Proc., 5 (2018) 22221–22228.
[16] G. Balakrishnan, R. Velavan, K. Mujasam Batoo, E.H. Raslan, Microstructure, optical and photocatalytic properties of MgO nanoparticles, Results Phys., 16 (2020) 103013, doi: 10.1016/j.rinp.2020.103013.
[17] K. Karthik, S. Dhanuskodi, C. Gobinath, S. Prabukumar, S. Sivaramakrishnan, Fabrication of MgO nanostructures and its efficient photocatalytic, antibacterial and anticancer performance, J. Photochem. Photobiol., B, 190 (2019) 8–20.
[18] N. Salehifar, Z. Zarghami, M. Ramezani, A facile, novel and low-temperature synthesis of MgO nanorods via thermal decomposition using new starting reagent and its photocatalytic activity evaluation, Mater. Lett., 167 (2016) 226–229.
[19] R. Sathyamoorthy, K. Mageshwari, S.S. Mali, S. Priyadharshini, P.S. Patil, Effect of organic capping agent on the photocatalytic activity of MgO nanoflakes obtained by thermal decomposition route, Ceram. Int., 39 (2013) 323–330.
[20] B. Benalioua, M. Mansour, A. Bentouami, B. Boury, E.H. Elandaloussi, The layered double hydroxide route to Bi–Zn co-doped TiO_2 with high photocatalytic activity under visible light, J. Hazard. Mater., 288 (2015) 158–167.
[21] F.-t. Li, X.-j. Wang, Y. Zhao, J.-x. Liu, Y.-j. Hao, R.-h. Liu, D.-s. Zhao, Ionic-liquid-assisted synthesis of high-visible-light-activated N–B–F-tri-doped mesoporous TiO_2 via a microwave route, Appl. Catal., B, 144 (2014) 442–453.

[22] L.M. Pastrana-Martínez, S. Morales-Torres, A.G. Kontos, N.G. Moustakas, J.L. Faria, J.M. Doña-Rodríguez, P. Falaras, A.M.T. Silva, TiO_2, surface modified TiO_2 and graphene oxide-TiO_2 photocatalysts for degradation of water pollutants under near-UV/Vis and visible light, Chem. Eng. J., 224 (2013) 17–23.
[23] J. Han, G. Zhu, M. Hojamberdiev, J. Peng, X. Zhang, Y. Liu, B. Ge, P. Liu, Rapid adsorption and photocatalytic activity for Rhodamine B and Cr(VI) by ultrathin BiOI nanosheets with highly exposed {001} facets, New J. Chem., 39 (2015) 1874–1882.
[24] C. Chang, H.-C. Yang, N. Gao, S.-Y. Lu, Core/shell p-BiOI/n-β-Bi_2O_3 heterojunction array with significantly enhanced photoelectrochemical water splitting efficiency, J. Alloys Compd., 738 (2018) 138–144.
[25] Y. Yang, Z. Zeng, C. Zhang, D. Huang, G. Zeng, R. Xiao, C. Lai, C. Zhou, H. Guo, W. Xue, M. Cheng, W. Wang, J. Wang, Construction of iodine vacancy-rich BiOI/Ag@AgI Z-scheme heterojunction photocatalysts for visible-light-driven tetracycline degradation: transformation pathways and mechanism insight, Chem. Eng. J., 349 (2018) 808–821.
[26] M. Gotić, S. Popović, S. Musić, Influence of synthesis procedure on the morphology of bismuth oxide particles, Mater. Lett., 61 (2007) 709–714.
[27] N. Motakef-Kazemi, M. Yaqoubi, Green synthesis and characterization of bismuth oxide nanoparticle using *Mentha pulegium* extract, Iran J. Pharm. Res., 19 (2020) 70–79.
[28] M. Ahila, M. Malligavathy, E. Subramanian, D.P. Padiyan, Controllable synthesis of α and β-Bi_2O_3 through anodization of thermally evaporated bismuth and its characterization, Solid State Ionics, 298 (2016) 23–34.
[29] A. Sadeghzadeh-Attar, Efficient photocatalytic degradation of methylene blue dye by SnO_2 nanotubes synthesized at different calcination temperatures, Sol. Energy Mater. Sol. Cells, 183 (2018) 16–24.
[30] C. Liang, J. Ma, Y. Cao, T. Zhang, C. Yang, Y. Wu, H. Li, H. Xu, Y. Hua, C. Wang, Adsorption of BiOBr microspheres to Rhodamine B and its influence on photocatalytic reaction, Chemosphere, 304 (2022) 135320, doi: 10.1016/j.chemosphere.2022.135320.
[31] T.A. Gadhi, A. Hernández-Gordillo, M. Bizarro, P. Jagdale, A. Tagliaferro, S.E. Rodil, Efficient α/β-Bi_2O_3 composite for the sequential photodegradation of two-dyes mixture, Ceram. Int., 42 (2016) 13065–13073.
[32] C. Wang, C. Shao, Y. Liu, L. Zhang, Photocatalytic properties BiOCl and Bi_2O_3 nanofibers prepared by electrospinning, Scr. Mater., 59 (2008) 332–335.
[33] D. Teng, J. Qu, P. Li, P. Jin, J. Zhang, Y. Zhang, Y. Cao, Heterostructured α-Bi_2O_3/BiOCl nanosheet for photocatalytic applications, Nanomaterials (Basel), 12 (2022) 3631, doi: 10.3390/nano12203631.
[34] K.K. Bera, M. Chakraborty, M. Mondal, S. Banik, S.K. Bhattacharya, Synthesis of α-β Bi_2O_3 heterojunction photocatalyst and evaluation of reaction mechanism for degradation of RhB dye under natural sunlight, Ceram. Int., 46 (2020) 7667–7680.
[35] K.K. Bera, R. Majumdar, M. Chakraborty, S.K. Bhattacharya, Phase control synthesis of α, β and α/β Bi_2O_3 hetero-junction with enhanced and synergistic photocatalytic activity on degradation of toxic dye, Rhodamine-B under natural sunlight, J. Hazard. Mater., 352 (2018) 182–191.
[36] R. Chen, Z.-R. Shen, H. Wang, H.-J. Zhou, Y.-P. Liu, D.-T. Ding, T.-H. Chen, Fabrication of mesh-like bismuth oxide single crystalline nanoflakes and their visible light photocatalytic activity, J. Alloys Compd., 509 (2011) 2588–2596.
[37] S.-J. Xia, F.-X. Liu, Z.-M. Ni, J.-L. Xue, P.-P. Qian, Layered double hydroxides as efficient photocatalysts for visible-light degradation of Rhodamine B, J. Colloid Interface Sci., 405 (2013) 195–200.
[38] M. Shao, J. Han, M. Wei, D.G. Evans, X. Duan, The synthesis of hierarchical Zn–Ti layered double hydroxide for efficient visible-light photocatalysis, Chem. Eng. J., 168 (2011) 519–524.
[39] H.F. Lin, R. Ravikrishna, K. Valsaraj, Reusable adsorbents for dilute solution separation. 6. Batch and continuous reactors for the adsorption and degradation of 1,2-dichlorobenzene from dilute wastewater streams using titania as a photocatalyst, Sep. Purif. Technol., 28 (2002) 87–102.
[40] J. Cunningham, G. Al-Sayyed, Factors influencing efficiencies of TiO_2-sensitised photodegradation. Part 1.—substituted benzoic acids: discrepancies with dark-adsorption parameters, J. Chem. Soc. Faraday Trans., 86 (1990) 3935–3941.
[41] L. Lin, M. Huang, L. Long, Z. Sun, W. Zheng, D. Chen, Fabrication of a three-dimensional BiOBr/BiOI photocatalyst with enhanced visible light photocatalytic performance, Ceram. Int., 40 (2014) 11493–11501.
[42] J. Li, F. Yang, Q. Zhou, L. Wu, W. Li, R. Ren, Y. Lv, Visible-light photocatalytic performance, recovery and degradation mechanism of ternary magnetic Fe_3O_4/BiOBr/BiOI composite, RSC Adv., 9 (2019) 23545–23553.
[43] S. Gao, C. Guo, S. Hou, L. Wan, Q. Wang, J. Lv, Y. Zhang, J. Gao, W. Meng, J. Xu, Photocatalytic removal of tetrabromobisphenol A by magnetically separable flower-like BiOBr/BiOI/Fe_3O_4 hybrid nanocomposites under visible-light irradiation, J. Hazard. Mater., 331 (2017) 1–12.
[44] P. Jha, K. Singh, Effect of field strength and electronegativity of CaO and MgO on structural and optical properties of SiO_2-K_2O-CaO-MgO glasses, Silicon, 8 (2016) 437–442.
[45] S.P. Pattnaik, A. Behera, S. Martha, R. Acharya, K. Parida, Facile synthesis of exfoliated graphitic carbon nitride for photocatalytic degradation of ciprofloxacin under solar irradiation, J. Mater. Sci., 54 (2019) 5726–5742.
[46] A. Behera, D. Kandi, S. Mansingh, S. Martha, K. Parida, Facile synthesis of $ZnFe_2O_4$@RGO nanocomposites towards photocatalytic ciprofloxacin degradation and H_2 energy production, J. Colloid Interface Sci., 556 (2019) 667–679.
[47] J. Li, Q. Zhou, F. Yang, L. Wu, W. Li, R. Ren, Y. Lv, Uniform flower-like BiOBr/BiOI prepared by a new method: visible-light photocatalytic degradation, influencing factors and degradation mechanism, New J. Chem., 43 (2019) 14829–14840.
[48] L. Yosefi, M. Haghighi, S. Allahyari, Solvothermal synthesis of flowerlike p-BiOI/n-$ZnFe_2O_4$ with enhanced visible light driven nanophotocatalyst used in removal of acid orange 7 from wastewater, Sep. Purif. Technol., 178 (2017) 18–28.
[49] S. Wang, Y. Guan, L. Wang, W. Zhao, H. He, J. Xiao, S. Yang, C. Sun, Fabrication of a novel bifunctional material of BiOI/Ag_3VO_4 with high adsorption–photocatalysis for efficient treatment of dye wastewater, Appl. Catal., B, 168 (2015) 448–457.